8.1 A Preliminary Study of Surface Temperature Cold Bias in COAMPS

Hung-Neng S. Chin, Martin J. Leach, Gayle A. Sugiyama and Fernando J. Aluzzi

Atmospheric Sciences Division
Lawrence Livermore National Laboratory
Livermore, California

1. INTRODUCTION

It is well recognized that the model predictability is more or less hampered by the imperfect representations of atmospheric state and model physics. Therefore, it is a common problem for any numerical models to exhibit some sorts of biases in the prediction. In this study, the emphasis is focused on the cold bias of surface temperature forecast in Naval Research Laboratory's three-dimensional mesoscale model, COAMPS (Coupled Ocean/Atmosphere Mesoscale Prediction System).

Based on the comparison with the ground station data, there were two types of ground temperature cold biases identified in LLNL (Lawrence Livermore National Laboratory) operational forecasts of COAMPS over the California and Nevada regions during the 1999 winter and the 2000 spring. The first type of cold bias appears at high elevation regions covered by snow, and its magnitude can be as large as 30 °F - 40 °F lower than observed. The second type of cold bias mainly exists in the snow-free clear-sky regions, where the surface temperature is above the freezing point, and its magnitude can be up to 5 °F - 10 °F lower than observed. These cold biases can affect the low-level stratification, and even the diurnal variation of winds in the mountain regions, and therefore impact the atmospheric dispersion forecast.

The main objective of this study is to explore the causes of such cold bias, and to further the improvement of the forecast performance in COAMPS. A series of experiments are performed to gauge the sensitivity of the model forecast due to the physics changes and large-scale data with various horizontal and vertical resolutions.

2. MODEL AND INITIALIZATION

COAMPS consists of a data assimilation system, a nonhydrostatic atmospheric forecast model, and a hydrostatic ocean model. For real-data simulations, COAMPS can use a complete atmospheric data assimilation system that is comprised of data quality control, analysis, and initialization. The initialization of COAMPS for real-data simulations is based on the NOGAPS (Navy Operational Global Atmospheric Prediction System) global-scale analysis fields, which have a resolution of 1°. The capability of using additional global- (AVN; 1°) or continental-scale analysis fields (ETA; 40-km) is also available in the LLNL version of COAMPS.

The atmospheric forecast model of COAMPS contains a compressible form of the dynamics. This model has nest-grid capability and flexible options for the model physics. The model physics includes parameterizations of subgrid-scale cumulus clouds (Kain and Fritsch 1993), explicit ice microphysics (Rutledge and Hobbs 1983), shortwave (SW) and longwave (LW) radiation (Harshvardhan et al. 1987), subgrid-scale mixing (Mellor and Yamada 1982), surface momentum and heat fluxes (Louis et al. 1982), and soil layer heat flux (Deardorff 1978). Runoff effects of surface precipitation and snow melting are considered in the surface energy equation via the ground wetness. COAMPS also employs a terrain-following vertical coordinate to simulate atmospheric phenomena over the complex terrain, and uses a time-splitting technique to minimize the time-step restriction of sound waves in the nonhydrostatic, compressible model. The reader is referred to Hodur (1997) for further details of COAMPS.

In this study, COAMPS is set up to contain 31 grid points in the vertical, with the grid spacing varied to maximize the resolution at lower levels. The grid spacing of the lowest layer is 0.02 km with each successive layer gradually increased to 1 km at 4.3 km, and then it becomes uniform at the resolution of 1 km between 4.3 km and 8.3 km in height. The grid size aloft is further reduced to 0.75 km between 8.3 km and 12.8 km. Above 12.8 km, the grid spacing is rapidly increased to 7.5 km with the domain top residing at 34.8 km. In the horizontal, two nested grids are used to achieve higher resolution for the areas of interest. The outer domain contains 91 x 73 grids and has a uniform grid spacing of 36 km. A grid size ratio of 3 is used to define the inner nested domain, which includes 73 x 91 grids and has a grid spacing of 12 km.

The rigid boundary condition is imposed at the vertical boundaries. A sponge-damping layer is placed above 11.3 km to minimize the reflection of internal gravity waves off the rigid upper boundary. The Davies (1976) boundary condition is applied to the lateral boundaries with a nudging zone of seven grid points at each lateral boundary. Constant time steps of 90 and 45 seconds for non-sound- and sound wave calculations, respectively, are used in the coarser grids for the time-splitting scheme. The time steps for the fine-grid domain are derived proportionally to the nest-grid size ratio. A time filter with a coefficient of 0.2 is applied to control computational instability associated with the leapfrog time approximation in the model.

A California winter precipitation case, occurring on January 21, 2000, is chosen for this study. Most of the simulations shown in this study use the NOGAPS data to drive the COAMPS model, except for two experiments, that use the ETA data. Various large-scale data are used to assess their impacts on the model forecast. A constant

Corresponding author address: Dr. H.-N. S. Chin, P. O. Box 808 (L-103), Livermore, CA 94551.

concentration of carbon dioxide at 300 PPM and an ozone profile from the NOGAPS climatology data are also used for radiation calculation.

The global data set of NOGAPS contains the data for both surface and pressure levels. The pressure-level data are available at twenty levels (i.e., 10, 20, 30, 50, 70, 100, 150, 200, 250, 300, 400, 500, 700, 800, 850, 900, 925, 950, 975, and 1000 mb), and are used to calculate the tendency terms of input data at the lateral boundaries. However, the hardwiring setting of the multivariate optimum interpolation in the data assimilation system forces the initial conditions to be computed from 16 pressure levels (i.e., excluding 800, 900, 950, and 975 mb). To concentrate on the impact of model physics on the COAMPS forecast, we adopt the so-called cold-start approach in this study (i.e., without using the data assimilation mode). In these cold-start simulations, only sixteen pressure levels are used to derive the initial conditions, except for two simulations, that include four additional pressure levels to examine the influence of vertical resolution of the large-scale data on the surface temperature forecast. The ETA data are available in an interval of 25 mb between 1000 mb and 100 mb along with two additional levels at 50 mb and 70 mb (i.e., totally 39 levels). However, only those pressure levels in common with the NOGAPS data are used in this study to gauge the impact of horizontal resolution of the large-scale data on the forecast performance.

3. EXPERIMENTS AND DESIGN

The experiments are designed to explore the cause of surface cold biases in COAMPS. Using the version 2.0.15 of COAMPS, a total of fifteen simulations are conducted in this study based on the changes of seven parameters. These parameters include the type of large-scale data, diagnosed cloud fraction in radiation transfer, surface snow albedo, surface snow melting and heat capacity of the snow surface, calling frequency of radiation transfer, relaxation time of the soil-layer heat flux, and the subjective adjusted factor for the climatology value of snow depth (see Table 1).

Results shown are focused on the simulations from the inner nest grids covering California and Nevada. The coverage of this finer-grid domain along with the topography, determined from the Silhouette terrain method, is shown in Fig. 1. The letters, A to F, mark the grid locations representing clear, cloudy, and mountain regions, respectively, in the sensitivity tests shown in Section 4.

The change of model physics in Exp1 is due to the deficiencies of Exp2 in both SW and LW radiation transfers. These deficiencies include (1) the diagnosed cloud optical properties due to the decoupled cloud fraction calculation with the model predicted stable cloud, and (2) treating the whole model grid columns in all either clear or cloudy condition. The second aspect would degrade the forecast performance under the partial cloudy condition within the whole model domain. The modified radiation scheme in Exp1 is able to improve the diagnosed cloud optical properties, and enables individual grid column to be in the either clear or cloudy condition.

Table 1. Design of numerical simulations. * indicates the simulations using 4 additional pressure levels at 800, 900, 950 and 975 mb to compute the initial conditions.

Simulation	Data Type	Radiation	Sfc Snow Albedo	Sfc Snow Melting	dtrad	Trelax	SNWP Adj Factor
Exp1	NOGAPS	LLNL	NRL	NRL	3600	96	1.0
Exp2	NOGAPS	NRL	NRL	NRL	3600	96	1.0
Exp3	NOGAPS	LLNL	LLNL	NRL	3600	96	1.0
Exp4	NOGAPS	LLNL	NRL	NRL	600	96	1.0
Exp5	NOGAPS	LLNL	NRL	NRL	3600	24	1.0
Exp6	NOGAPS	LLNL	NRL	NRL	3600	384	1.0
Exp7	NOGAPS	LLNL	LLNL	NRL	1200	96	1.0
Exp8	NOGAPS	LLNL	LLNL	NRL	1200	48	1.0
Exp9	NOGAPS	LLNL	LLNL	NRL	1200	24	1.0
Exp10	ETA	LLNL	LLNL	NRL	1200	24	1.0
Exp11	NOGAPS	LLNL	LLNL	NRL	1200	24	0.5
Exp12	NOGAPS	LLNL	LLNL	NRL	1200	24	1.0
Exp13	NOGAPS	LLNL	LLNL	LLNL	1200	24	0.5
Exp14	NOGAPS*	LLNL	LLNL	LLNL	1200	24	0.5
Exp15	ETA*	LLNL	LLNL	LLNL	1200	24	0.5

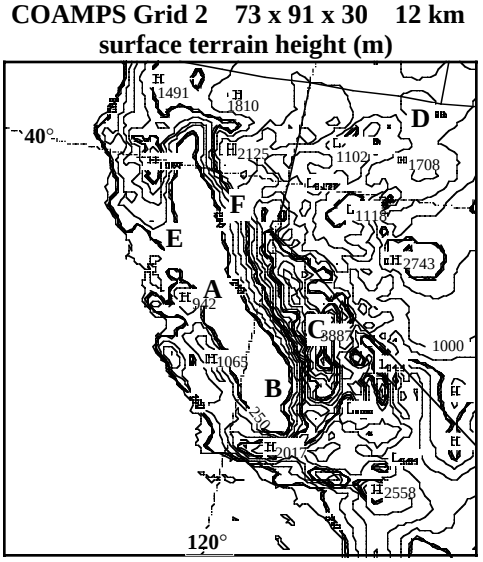

Fig. 1. The topography used in this study is given from the Silhouette terrain method.

The experiment of Exp3 is used to gauge the impact of surface snow albedo on the ground temperature

forecast. In NRL's surface albedo (α) calculation, the adjusted surface albedo (α') due to the presence of snow is defined as

$$\alpha' = \alpha + k \bullet (\alpha_{snow} - \alpha), \quad (1)$$

where k = min(snow_depth/100 mm, 1.0). This equation assumes that the snow albedo is equal to α_{snow} (i.e., 0.84) as the accumulated snow depth is greater than 100 mm. According to Eq. (1), the adjusted surface albedo with small snow depth can increase rapidly to a very large value close to α_{snow} in several numerical time steps even without changing the snow depth. Once the adjusted surface albedo reaches α_{snow}, Equation (1) will lead to a fixed surface albedo at α_{snow} throughout the simulation. As a result, the daytime ground temperature can be greatly underestimated due to this runaway effect of surface snow albedo in reducing the net downward solar radiation.

To improve this snow albedo parameterization, the adjusted surface albedo in Exp3 is expressed by

$$\alpha' = \max(k' \bullet \alpha_{snow}, \alpha), \quad (2)$$

where k' = min(snow_depth/dd, 1.0). dd in Eq. (2) is set to 100.0 / 150.0 mm as the ground temperature is below / above the freezing point. The temperature dependence of dd is used to account for the smaller albedo for older and polluted snow in the warmer condition as shown in the observations (Pielke 1984).

The experiment Exp4 is used to assess the quantitative impact of the calling time interval of the radiation calculation. Due to the computational restriction, radiation physics is practically computed in a fixed number of time steps in numerical models. Therefore, the radiation effect at every grid column within each calling time interval is assumed the same as the one using the value calculated at the latest call of the radiation scheme. As a result, this would lead to underestimation / overestimation of net downward SW radiation flux during the first / second half of daytime, and thus produce a cold / warm bias of predicted ground temperature at the corresponding stage. Similar bias of nighttime LW net upward flux would also occur in the use of finite calling time interval (dtrad). As compared to its counterpart computed at every time step, the fixed dtrad acts to cause a temporal lag of calculated radiation flux. This bias can be reduced by using a reasonably small calling interval. In addition, the simulation using a smaller dtrad would particularly be suitable for the short-lived cloudy condition (i.e., cloud lifetime < dtrad).

The experiments of Exp1, Exp5 and Exp6 are mainly used to study the systematic cold bias of ground temperature at the locations with lower elevation. The possible cause of this cold bias is attributed to the heat flux parameterization of the soil layer in the surface energy equation, where the ground temperature (T_g) tendency term is expressed by

$$\frac{\partial T_g}{\partial t} = \bullet\bullet\bullet\bullet - \frac{1}{T_{relax}} (T_g - T_{soil}). \quad (3)$$

In Eq. (3), T_{relax} is the relaxation time of the nudging constant, and T_{soil} a fixed deep soil temperature given from the climatology value.

To compromise the accuracy and the computational efficiency of the radiation calculation, a medium size of calling time interval at 1200 seconds is used for the rest of sensitivity experiments. As in Exp1, Exp5, and Exp6, Exp7, Exp8 and Exp9 are used to gauge the soil-layer heat flux impact at smaller calling time interval of the radiation calculation.

The impact of different large-scale data on the COAMPS forecast is shown in Exp10 using the ETA data. To further the understanding of the substantially large surface cold bias in the high elevation regions, a subjective adjusted factor for the climatology value of snow depth is used to represent the proper initial condition for surface snow. This impact is shown in Exp11 based on the observed snowfall data at the ground stations.

The impacts of snow heat capacity and snow melting physics on the surface energy equation are studied in Exp12. In NRL's formulation, the land surface with the accumulated snow depth less than 30 mm is treated as the snow-free surface. Otherwise, it is considered as the snow surface. The heat capacity of land surface is expressed by

$$C_{snow-free} = 42000 \bullet \sqrt{27.5 \bullet [0.387 + 0.15 \bullet gwet \bullet (1 + gwet)]}, \quad (4)$$

or

$$C_{snow} = 0.001 \bullet 1925600 \bullet \min(snow\_depth, 500mm). \quad (5)$$

Besides, the effect of surface snow melting is not calculated as a part of the surface energy equation. This effect is computed after the first guess of surface temperature is given from the surface energy equation and assumes that the final surface temperature is fixed at the freezing point when the melting occurs.

To improve the transition impact of snow-free to snow surface on the ground temperature, a revised treatment of surface snow effect is proposed in Exp12. The revised heat capacity of snow surface is based on Eq. (4) for both snow-free and snow surfaces, while the upper limit of ground wetness (gwet) in the snow case is set to a larger value (0.98) than its snow-free counterpart (0.6). Meanwhile, the snow melting effect is considered as a part of the surface energy equation. Therefore, the surface temperature can be warmer than the freezing point when the surface snow depth is not substantially large.

The sensitivity experiments aforementioned also act to define an experiment with the optimum configuration of physics option (Exp13), that could improve the surface cold bias of COAMPS forecast. Similar to Exp13, two additional experiments (Exp14 and Exp15) are performed to study the impact of vertical and horizontal resolutions of large-scale data.

All simulations shown in this study use the same terrain data that are determined from the Silhouette method. The parameters to derive these terrain data are listed as follows; nsrch = 4, iwvlng = 2, topores = 1.0, silwgt = 0.5, and silmax = 0.5. These simulations are also used to compare with the ground station data to quantify the role of individual factor on the model performance.

4. RESULTS

Due to the focus of this study, results shown are primarily concentrated on the comparisons of surface fields among the sensitivity experiments. All simulations start from 00 GMT, January 21, 2000, and last for 24 hours of physical time to predict a full diurnal cycle. The initial conditions of this study given from the NOGAPS data indicate that a NW-SE oriented low pressure zone is located near the middle of model domain with two prominent cyclonic circulations centered near the Yuba City and the Granite mountains, respectively. The coldest temperature of 21 °F or so exists near the southern end of the Sierra Nevada. Another evident cold region with the minimum of 32 °F or so is located near the middle of the northern boundary (Fig 2a). The initial condition of surface snow depth is given from the climatology values, which clearly show two major maximum zones to coincide with the minimum temperature distributions (Fig. 2b).

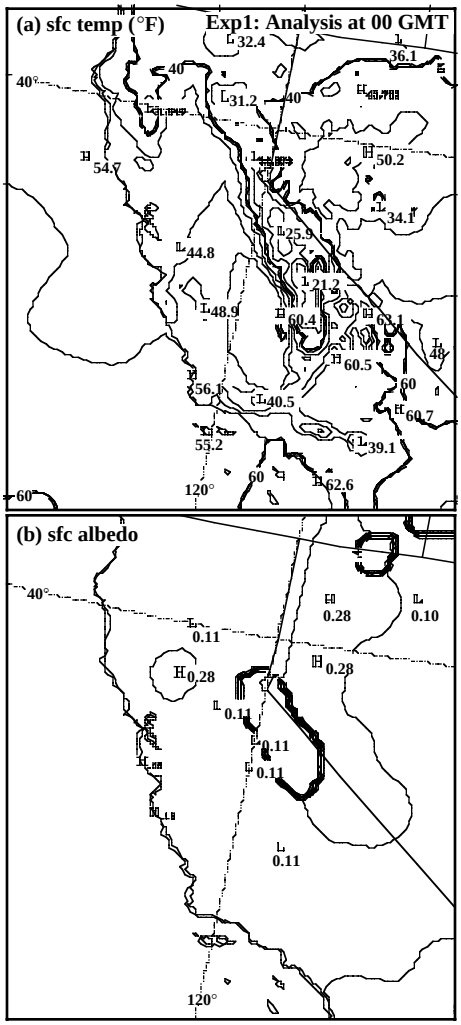

Fig. 2. Horizontal cross-sections of initial conditions for the experiment of Exp1. (a) Surface temperature, and (b) Surface albedo.

Results of Exp1 exhibits a clear coupling between the diagnosed cloud fraction and the model predicted cloud activity, while the cloud fraction in Exp2 covers a much wider area than the predicted cloud coverage (not shown). As a result, the radiation transfer update in Exp1 can influence not only the surface, but also the whole atmosphere, and thereby alters both the surface energy budget and grid-column stratification.

In contrast to this radiation effect, the impact of modified surface albedo calculation in Exp3 is primarily focused on the surface level. Therefore, the wind and precipitation forecasts of Exp3 are almost identical to their counterparts in Exp1. However, the improved surface albedo forecast (Fig. 3) effectively prevents the surface temperature from being overwhelmingly cooled down over the snow cover regions. Thus, the warmer ground temperature (up to 10 °F) in Exp1 enables the snow to melt more and to reduce the spatial coverage of the snow pack.

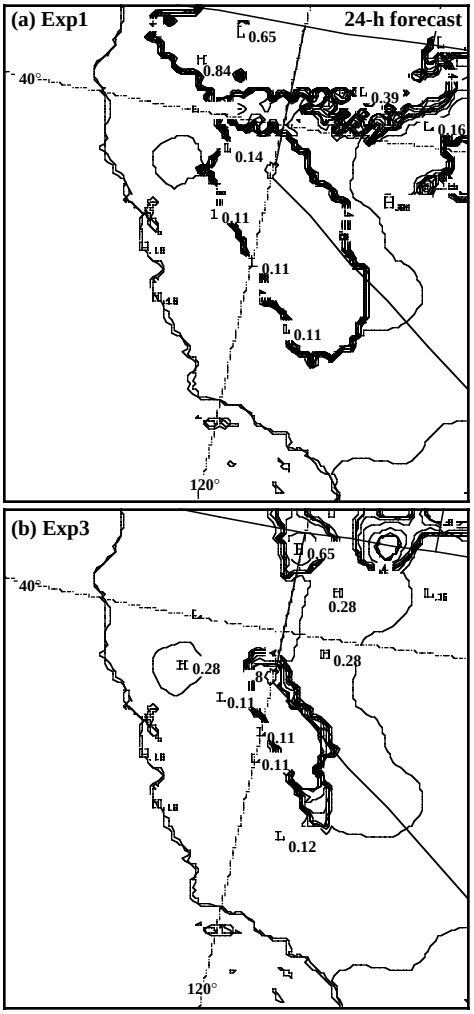

Fig. 3. Horizontal cross-sections of surface albedo for the simulations at 24 hours. (a) Exp1, and (b) Exp3.

The experiments of Exp4, Exp5, Exp6, Exp7, Exp8, and Exp9 are used to gauge the influence of dtrad and Trelax on the overall characteristics of model forecasts. Results indicate that the shorter radiation calling time interval (dtrad= 600 vs. 3600 seconds) acts to accelerate the evolution of predicted surface temperature in all atmospheric conditions as marked at the locations shown in Fig. 1. This impact can lead to a warming in the morning and earlier afternoon (e.g., up to 5 °F in the

clear-sky condition), and a cooling (1 °F or less) in the late afternoon and the evening (not shown). Our results further show that the shorter relaxation time (i.e., 24 hours) in all atmospheric conditions acts to warm the surface more effectively, particularly during the night (not shown). These findings are also seen in the simulations with medium size of dtrad (i.e., 1200 seconds).

The ground station data of 2-m temperature at six locations are used to validate the model results. These locations include Sacramento and Fresno in the Central Valley, Monterey and Los Angeles in the coastal region, and Reno and Truckee in the mountain region.

Further comparisons are conducted using various large-scale data (i.e., NOGAPS in Exp9 vs. ETA in Exp10) under the same vertical resolutions. Results indicate that the use of ETA data does not substantially improved the model forecast even for the location with better initial temperature at Sacramento. More noticeable differences of surface temperature appear to occur near the coastline, such as Monterey and Los Angeles. This may suggest that the small-scale horizontal variation near the coastline may introduce an additional uncertainty to the model forecast. As a whole, the largest cold bias still exists at the high elevation locations.

To further the understanding on the cause of the coldest bias in the mountain region, reduced initial snow amount via a subjective adjusted factor of 0.5 and modified snow melting physics are gauged in Exp11 and Exp12. The reduced snowfall in Exp11 is chosen based on the observations in the Sierra Nevada, which were lower than the climatology by a factor ranging from 40% to 60% among the stations. As compared to Exp9, the reduced surface snow amount in Exp11 can increase the daytime near-surface temperature by up to 4 °F at the high elevation locations. Nonetheless, this enhanced daytime predicted surface temperature is still far below the observation by up to 14 °F. Further results in Exp12 indicate that unlike the capped daytime surface temperature (i.e., at the freezing point) at Reno in Exp9, the modified snow melting parameterization allows this temperature to rise above the freezing point by up to 2 °F when the snow depth is not substantially large.

Using the optimum setting of physics options determined from the sensitivity experiments above, Exp13, and Exp14 and Exp15 are performed to gauge the vertical-resolution impact of the large-scale data. These comparisons also include the observations and the first three sensitivity experiments to quantify the impact of modified radiation transfer and snow albedo calculation at selected locations. Their results are summarized in Fig. 4.

The over-predicted cloud fraction in the Central Valley of Exp2 would cause nighttime warming and daytime cooling relative to their counterparts in Exp1 as a result of the trapping of upward LW flux and the shading of downward SW flux, respectively (Figs. 4a and 4b). This cloud fraction impact also appears in the coastal region (Figs. 4c and 4d). In addition, the runaway effect of surface snow albedo on the temperature field is substantially improved in Exp3 at the location with small snow depth, where the daytime surface temperature is noticeably warmed up (Fig. 4e). However, this impact is negligibly small at the location with large snow depth (Fig. 4f). As a whole, the predicted surface temperature of these three experiments is still far below the observations in the mountain region.

With the optimum setting of physics options, the simulated surface temperature in Exp13 appears to improve significantly at all locations. As compared to Exp1, the improved daytime surface temperature of Exp13 at high elevation stations is still halfway below the observations (Figs. 4e and 4f). However, the resulting low-level winds at the uphill side of the Sierra Nevada clearly exhibit the diurnal variation (not shown). The additional pressure-level data near the surface in Exp14 and the use of other large-scale data with finer horizontal resolution in Exp15 do not substantially further the improvement of surface cold bias prediction for the case of concern.

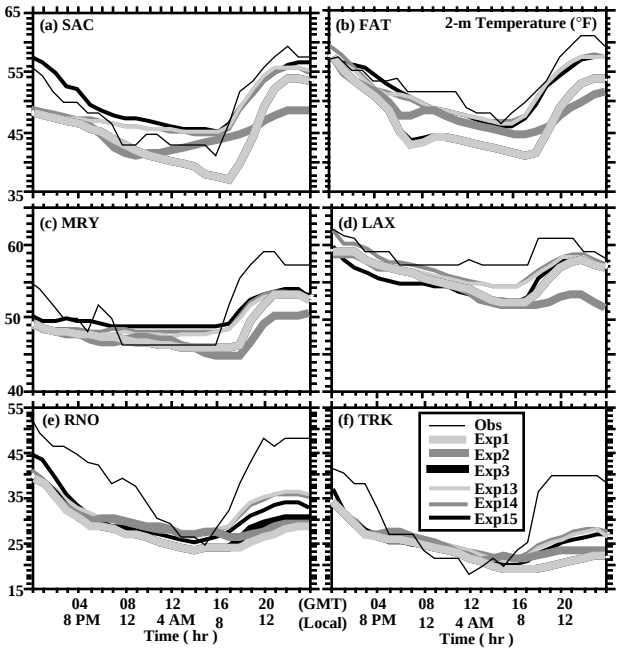

Fig. 4. Time series of 2-m temperature at six ground stations for Exp1, Exp2, Exp3, Exp13, Exp14, and Exp15. (a) Sacramento, (b) Fresno, (c) Monterey, (d) Los Angeles, (e) Reno, and (f) Truckee.

5. SUMMARY AND DISCUSSION

A modified version of NRL's three-dimensional mesoscale model is used to study the systematic cold bias of surface temperature forecast in COAMPS. A California winter precipitation case, occurring on January 21, 2000, is used for this study. A series of experiments are performed to gauge the sensitivity of the model forecast to the physics changes and large-scale data with various horizontal and vertical resolutions. These simulations act to determine an optimum setting of physics options for the improvement of COAMPS surface temperature forecast. In this study, seven parameters are considered in the sensitivity tests. They include the changes in the large-scale data type, radiation transfer, the surface snow albedo parameterization, the

surface snow melting calculation, the calling frequency of radiation calculation, the nudging coefficient for the soil-layer heat flux, and the snow depth adjusted factor for the initial condition. Among these parameters, near half of them are contributed to the stronger cold bias at the locations with surface snow.

Simulations indicate that the cloud radiative properties of COAMPS and their corresponding shortwave and longwave fluxes have been greatly improved in the modified radiation transfer calculation. As a result, the diurnal variation of low-level winds can be simulated in the low elevation hill, where there is no surface snow. However, this diurnal variation is suppressed at the high elevation areas with surface snow due to its overwhelmingly cooling effect. The modified parameterization of surface snow albedo can further eliminate the drawback of this runaway character. Unlike the fixed surface temperature when snow melts the modified melting physics of surface snow enables the surface temperature to rise above the freezing point as melting occurs. In addition, the sensitivity tests show that both the shorter calling time interval of radiation calculation and smaller nudging coefficient of the soil-layer heat flux can help reduce the surface cold bias.

Results also demonstrate the need to improve the representation of the initial condition for the surface snow depth due to its strong impact on the surface temperature forecast. For simplicity, a constant subjective snow depth adjusted factor of the climatology value is used in this study to account for a better initial condition for the surface snow depth. The ultimate goal to lessen this impact is to use the large-scale data, which contain measured surface snow depth via the objective analysis like the temperature field. Up to date, this data set is, however, not available in any existing large-scale data so that a compromise approach may be taken by considering a snow depth adjusted factor, which has spatial dependence. To this end, more research effort is needed to obtain a more realistic representation of the snow depth adjusted factor.

As compared to the impact of physics change on the surface temperature forecast, it is worth pointing out that the use of finer horizontal and vertical resolutions of large-scale data from NOGAPS and ETA, respectively, exhibits little improvement to the simulated surface temperature at all geographic locations in this study. This finding should be taken with caution. More case studies at this aspect are needed to generalize this conclusion.

Overall speaking, the use of the optimum setting of physics options greatly improve the surface temperature forecast, while it still remains some degree of forecast uncertainty, particularly at the coastal and high elevation locations. The uncertainty near the coastline may be attributed to the sharp gradient of boundary layer properties between the ocean and near land. Therefore, smaller scale features tend to form near the ground. However, these subgrid-scale features cannot be resolved in most forecast models for the computational reason. This uncertainty may be weakened by using a finer grid resolution near the ground. On the other hand, the largest forecast uncertainty of this study appears at high elevation locations. Although the model resolved higher terrain (by 300 m or so) can contribute to certain degree of the surface cold bias (by 6 °F or so) via the initial condition. However, the magnitude of the cold bias contributed by terrain is still not large enough to be viewed as a predominant factor. Therefore, our results suggest that this high degree of uncertainty in the surface temperature forecast may be caused by the limited observations in the high elevation regions as a result of its degrading in the quality of initial conditions. Although fairly large cold bias still exists in the simulation using the optimum setting of physics options, the failure of simulating the diurnal variation of low-level winds in the mountain regions with surface snow has been successfully improved.

ACKNOWLEDGMENTS. The authors would like to thank NRL and Department of water resources, California for providing us the mesoscale model and the ground station snowfall data for this study. This work was supported by the Department of Energy (DOE) National Advisory Release Assessment Program and Chemical-Biological Non-Proliferation Program, and conducted under the auspices of the U. S. DOE by the Lawrence Livermore National Laboratory under contract No. W-7405-ENG-48.

REFERENCES:

Davies, H. C., 1976: A lateral boundary formulation for multi-level prediction models. *Quart. J. Roy. Meteor. Soc.*, **102**, 405-418.

Deardorff, J. W., 1980: Stratocumulus-capped mixed layers derived from a three-dimensional model. *Bound.-Layer Meteor.*, **18**, 495-527.

Harshvardhan, R. Davies, D. Randall, and T. Corsetti, 1987: A fast radiation parameterization for atmospheric circulation models. *J. Geophys. Res.*, **92**, 1009-1015.

Hodur, R., 1997: The Naval Research Laboratory's coupled ocean-atmospheric mesoscale prediction system (COAMPS). *Mon. Wea. Rev.*, **125**, 1414-1430.

Kain, J. S., and J. M. Fritsch, 1993: Convective parameterization for mesoscale models: The Kain-Fritsch scheme. *The Representation of Cumulus Convection in Numerical Models*, Meteor. Monogr., No. 46. Amer. Meteor. Soc., 165-170.

Louis, J. F., M. Tiedtke, and J. F. Geleyn, 1982: A short history of the operational PBL-parameterization at ECMWF. *Workshop on Planetary Boundary parameterization*, Reading, United Kingdom, ECMWF, 59-79.

Mellor, G. L., and T. Yamada, 1982: Development of a turbulence closure for geophysical fluid problems. *Rev. Geophys and Space Phys.*, **20**, 851-875.

Pielke, R. A., 1984: Mesoscale Meteorological Modeling. Academic Press, 612 pp.

Rutledge, S. A., and P V. Hobbs, 1983: The mesoscale and microscale structure of organization of clouds and precipitation in midlatitude cyclones. VIII: A model for the seeder-feeder process in warm-frontal rainbands. *J. Atmos. Sci.*, **40**, 1185-1206.